ARTICLE

Constructing Metal-Based Structures on Nanopatterned Etched Silicon

Xiaojiang Zhang, Yinghong Qiao, Lina Xu, and Jillian M. Buriak*

National Institute for Nanotechnology, 11421 Saskatchewan Drive, Edmonton, Alberta, Canada T6G 2M9, and the Department of Chemistry, University of Alberta, Edmonton, Alberta, Canada T6G 2G2

ABSTRACT Silicon surfaces with nanoscale etched patterns were obtained using polystyrene-*block*-poly(4-vinylpyridine) (PS-*b*-P4VP) block copolymer films as templates, followed by brief immersion in HF(aq). The resulting interfaces were comprised of pseudohexagonal arrays of pits on the silicon, whose shapes depended upon the chosen silicon orientation. The top unetched face of silicon remains capped by the native oxide, and the pit interiors are terminated by $Si-H_x$. Selective chemical functionalization *via* these two chemical handles was demonstrated to be a viable approach toward building nanostructured metal oxide and metal features within these silicon pits and on the top face. Using a series of interfacial chemical reactions, including oxidation (of $Si-H_x$-terminated regions), hydrosilylation, and alkoxysilane-based chemistry on silicon oxide, the growth of metal-based structures can be spatially controlled. In the first approach, titania nanobowls were grown within the etch pits, and in the second, galvanic displacement was used to produce gold nanoparticles either within the etch pits, on the top silicon face, or both.

KEYWORDS: silicon · surface patterning · etching block copolymers · self-assembly · titania · gold nanoparticles

Nanopatterning on semiconductor surfaces continues to attract a great deal of attention because of the myriad of practical applications in areas such as sensor design, catalysis, and electronic circuit devices, interfacing with objects of biological origin, and many others.[1−6] The two major patterning motifs, classified as either top-down or bottom-up, can be used to achieve nanoscale fabrication of features on a large variety of substrates.[7−9] Bottom-up strategies are often inspired by strategies similar to those found in Nature, in particular a self-assembly-based[10] or self-ordering[11,12] approach. Many classes of organic-based molecules are capable of forming higher order structures *via* self-assembly,[13−15] and synthetic block copolymers have, for the past 15 years, become the focus of a great deal of sub-100 nm patterning for semiconductor-based applications because of compatibility with existing silicon-based nanofabrication.[1,16] Block copolymers have enormous potential for self-assembly-based nanopatterning approaches due to the broad range of obtainable structures, tunable geometries, and synthetic accessibility.[1,16−30] A number of groups have been developing methods to harness the enormous potential of block copolymer self-assembly for directing spatially localized chemical reactions on surfaces.[9,31−37] In essence, the block copolymer acts as a template, and thus the nanoscale pattern of the self-assembled polymer can be transferred directly to the interface with which it makes contact.

One approach we have recently developed is a simple method to generate sub-100 nm etched patterns on silicon wafers using self-assembled block copolymer templates.[31] With a monolayer-thick block copolymer PS-*b*-P4VP film as the template material, silicon surfaces can be etched by HF(aq) to give a uniform, pseudohexagonal pattern, as shown in Figure 1. In addition to the nanoscale morphology produced by this approach, the interior of the pores have a different termination ($Si-H_x$) than the flat areas surrounding the pores, that retain their native oxide termination.[31] As a result, parallel functionalization strategies should be possible in which pore interiors could be modified separately from the surrounding areas, allowing for the generation of more sophisticated, higher order structures. In this paper, we demonstrate the synthesis of metal oxide- and metal-based nanostructures using the selectivity provided by these chemical handles within, and outside, the nanopore patterns. In a first iteration, titania nanostructures were grown within the pores, and in a second, the pores were utilized to guide the deposition of gold nanoparticles *via* galvanic displacement.

RESULTS AND DISCUSSION

As mentioned *vide supra*, the amphiphilic diblock copolymer, polystyrene-*block*-poly(4-vinyl pyridine), here referred to as PS-*b*-P4VP, self-assembles on interfaces to form a monolayer of hexagonal close-packed arrays of block copolymer micelles. These films

* Address correspondence to jburiak@ualberta.ca.

Received for review March 23, 2011 and accepted May 5, 2011.

Published online May 05, 2011
10.1021/nn201109s

© 2011 American Chemical Society

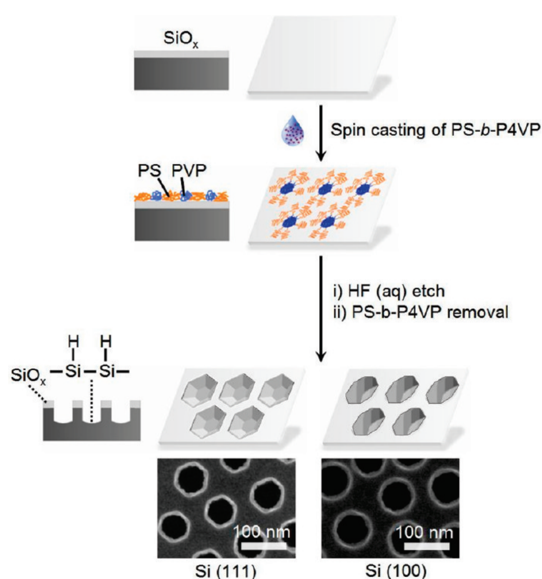

Figure 1. Schematic outline of the patterned etching process on silicon surfaces. Silicon substrates with native oxide on the surface were coated with a monolayer of a diblock copolymer, PS-*b*-P4VP, followed by HF etching and polymer removal procedure to produce the etched silicon surface.

were then used to generate nanoscale etching patterns on different types of silicon wafers, with (100), (111), and (110) orientations, as outlined in Figure 1 for the first two orientations.[31] The dimensions of the P4VP micellar core and PS shell are tunable through simple adjustment of the molecular weight of the commercially available block copolymers. Center-to-center spacings of hexagonal packed PS-*b*-PVP BCPs range from 16 to 290 nm,[31,38−42] and the PVP core diameters from 12 to 85 nm.[43] In this paper, the polymer chosen was PS-*b*-P4VP (M_n = 109 000-*b*-27 000 g/mol), which on silicon leads to hexagonal packing of micelles with center-to-center spacings of 110 nm. The silicon substrate coated with the block copolymer soft mask was then immersed in a dilute HF(aq) solution for a given time, and then the polymer film was removed through 5 min of ultrasonication in neat toluene. The block copolymer, PS-*b*-P4VP, contains pyridyl groups, which are protonated by HF(aq) to form poly(pyridinium) fluoride, which etches the silicon in an anisotropic fashion.[31] Etching takes place exclusively beneath the protonated P4VP cores of the polymer micelles, and the PS matrix in the copolymer film protects the native oxide on the silicon surfaces from the HF etching solution; the native oxide terminated silicon surfaces remain unetched (Figure 1). Because this etching is spatially selective, the interior chemical functionalities of the pores differ from those on the flat, top surface. This observation means that orthogonal chemical functionalization is possible, allowing for particular functionalization within the pore or on the unetched interface.

Formation of Titania Nanobowls. Monolayers of self-assembled block copolymers have been widely used to pattern oxide and semiconductor materials.[17,44−52] Because of the importance of titania nanostructures for a variety of applications, ranging from catalysis, sensors, and photovoltaics[53−57] to biomedical applications of silicon/titania micro- and nanopatterns,[58−61] we set out to use these ordered pit arrays on silicon as a template for the selective growth of periodic titania nanostructures.[62−67] As illustrated schematically in Figure 2a for the PS-*b*-P4VP block copolymer/HF(aq) etching, the pit interiors are Si−H_x terminated, and the top face of the silicon remains native oxide-capped. Exposure of the silicon sample to an alkylchlorosilane will result in selective silanization of the native oxide: Immersion of the sample in a 1.3 mM solution of octadecyltrichlorosilane (OTS) in dry hexanes for 30 min at room temperature led to formation of a hydrophobic monolayer on the top oxide region of the wafer.[68−71] Water contact angle measurements substantiate the high surface hydrophobicity (110.5°) after functionalization with the octadecylsilyl group; the water angles for the cleaned silicon wafer and the as-etched silicon wafer are 17° and 50°, respectively. While the array of pits on the surface will be expected to increase the hydrophobicity above that of a flat surface (since the interface is effectively roughened),[72−75] the measured water contact angle is indeed substantially higher than the prefunctionalized, freshly etched interface, as would be expected for this long alkyl chain termination. Immersion of the silanized sample in 30% (w/w) hydrogen peroxide(aq) overnight results in oxidation of the Si−H_x-terminated interfaces within the pore interiors, leading to a decrease in contact angle to ∼90°. The decrease in contact angle would be the result of conversion of the Si−H_x pit interiors to a more hydrophilic Si−OH termination following H_2O_2 oxidation.[76,77] The insulating organic monolayer formed in the previous silanization step is expected to be stable to these oxidizing conditions.[78,79] The samples, after removal from the aqueous H_2O_2 solution, were dried in air, and no attempt was made to dry them further (under vacuum, for instance), as the presence of residual water was required for the next step. Brief exposure of this silicon shard to $TiCl_4$(g) at 80 °C under 1 atm of nitrogen for 5 min results in the formation of amorphous titania on the surface of the substrate,[80] exclusively inside the etched pits. As water was present in the pit regions, the addition of $TiCl_4$ vapor presumably leads to the formation of a Ti−O−Ti network on these silica surfaces.[81−84] After TiO_2 deposition, the sample was rinsed with water and dried under a nitrogen gas stream. Finally, the sample was annealed at 550 °C in air for 3 h to form anatase TiO_2 and to remove the residual carbon-based polymers and the alkyl chains on the substrate surface.[85,86] XRD showed transformation of amorphous titania to anatase during calcination (Supporting Information, Figure S1).

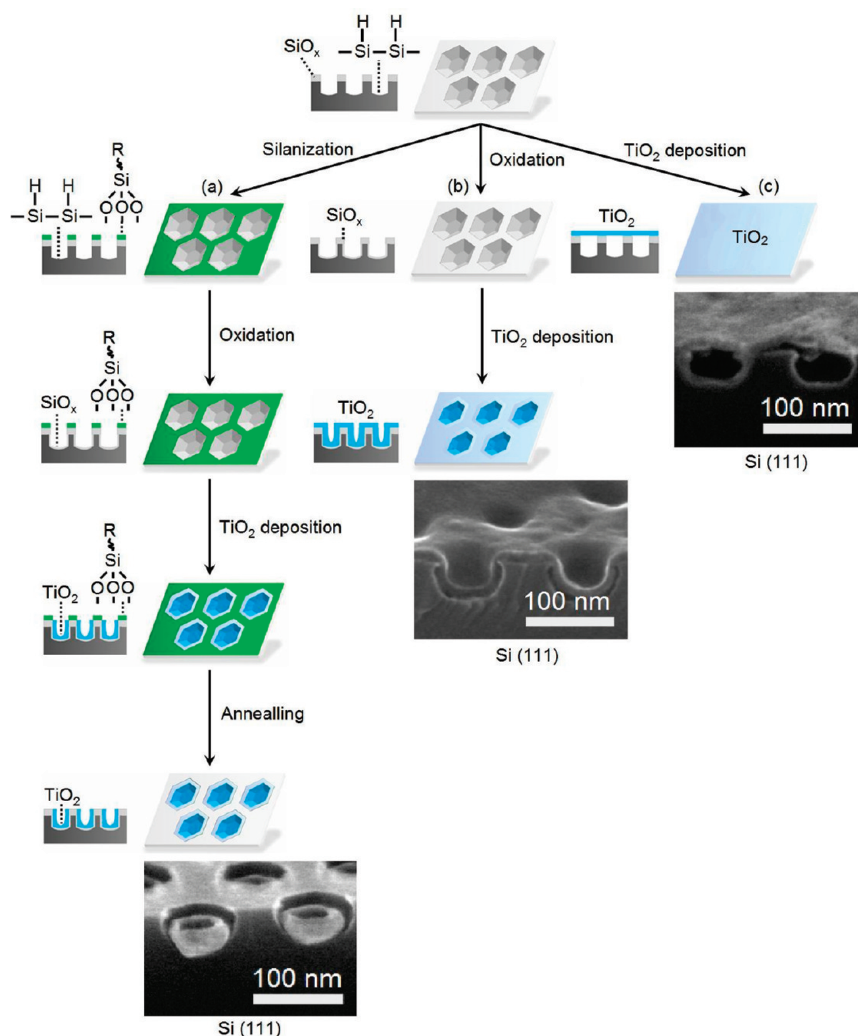

Figure 2. Schematic representation of titania growth on etched Si(111) surfaces. (a) Titania nanobowls formed inside the etched pits on silanized and oxidized silicon surfaces. (b) A titania film formed over the entire surface on a fully oxidized sample. (c) Titania formed exclusively on the native oxide of an as-etched silicon substrate.

Scanning electron microscope (SEM) images are shown in Figure 3 to visualize the structure of the etched silicon interfaces and of the titania nanobowl structures formed within them. As revealed in the plan view scanning electron microscopy image of the clean, freshly prepared silicon etch pits (Figures 3a,b), hexagonal pit shapes were observed on the Si(111) wafer surface, with etch pit depths of ~45 nm and a center-to-center pit separation of ~100 nm. Figure 3c−f shows SEM images of titania nanobowls. Typical dimensions of the titania nanobowls as fabricated were on average 55 ± 5 nm for the outer diameter (average of 40 measurements), ~40 nm for the inner hole diameter, and ~40 nm for the height. An average diameter of the inner hole and of the height could not be determined, as the shapes were often irregular. Side view SEM images are shown in Figure 3d−f, in which one can notice that the tops of these titania nanobowls were several nanometers lower than the level of the wafer surface. The elemental identities of the titania-loaded silicon wafers were verified by ~10 nm resolution scanning Auger microscopy (SAM, Supporting Information, Figure S2).

To demonstrate that the self-assembly of the OTS monolayer on the hybrid hydrophilic/hydrophobic silicon surfaces played a key role in the preferential deposition of titania, two control experiments were carried out, as illustrated in Figure 2b,c. In the first experiment, a freshly etched silicon surface was oxidized with hydrogen peroxide treatment [30% (w/w) H_2O_2, overnight] so that the entire surface was terminated by hydroxyl groups. Upon exposure to $TiCl_4$(g), a continuous ~20 nm titania film formed over the entire surface, as shown in Figure 3g, the thickness of which could be controlled by altering the deposition time (for two examples, see Figure S3). In the second experiment, the as-etched substrate was used directly in the titania deposition, as shown in Figure 3h. As stated earlier, following HF(aq) etching, the interior pit surfaces are Si−H_x-terminated, and as a result, no titania was observed inside the pits in the side view SEM images; only

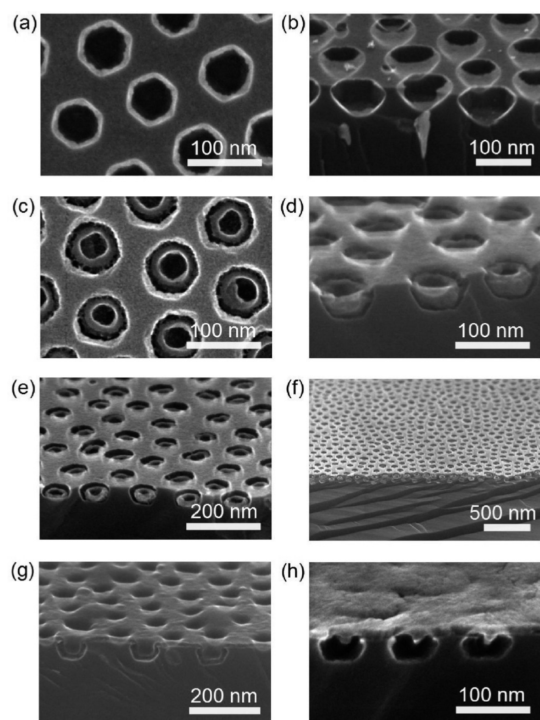

Figure 3. SEM images of (a and b) freshly etched Si(111) substrates, (c–f) titania nanobowls formed on etched silicon surfaces, (g) a titania film formed over the entire surface, which was fully oxidized, and (h) titania formed exclusively on the silicon native oxide interface.

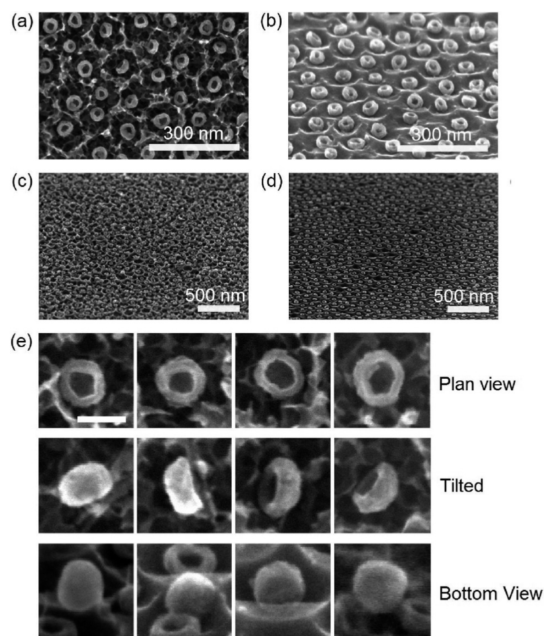

Figure 4. (a–d) SEM images of titania nanobowls on etched Si(111) surfaces released through exposure to dilute HF(aq). (e) SEM images of released titania nanobowls in various orientations.

the flat silicon native oxide surface was covered with the titania film.

In order to more fully analyze the titania nanobowls by electron microscopy, the silicon substrate was etched back with 0.02% HF(aq) for 6 h, as shown in Figure 4. Titania can be dissolved in acidic HF(aq) or a neutral fluoride-containing aqueous solution to form soluble $[TiF_6]^{2-}$ complexes,[87] but with this brief and dilute exposure, the nanostructures emerge intact.[45] If a higher concentration of HF(aq) is used, 5% for example, obvious damage to the titania nanobowls was observed (Figure S4, Supporting Information). The dilute HF(aq) etching was carried out to the point when the nanobowls are on the verge of total release into solution to allow for unencumbered SEM viewing of the structures in various configurations, including plan view, side view, and from the bottom. These images reveal that the nanobowls are apparently continuous throughout the entire bowl structure, including the bottom.

The TiO_2 nanobowls can be further functionalized with gold nanoparticles through a selective UV-mediated reaction that leaves the silica interfaces untouched. Using an aqueous 5×10^{-5} M $HAuCl_4$ solution that had been neutralized to pH 7 with a 10^{-3} M KOH(aq) solution, gold nanoparticles with a diameter of less than 4 nm were found exclusively on the titania nanobowls after a 5 min application of the 254 nm UV from a 5 W screen inspection UV lamp.[88–90] During the photocatalytic process, the photogenerated electrons on titania surfaces reduce Au(3+) to Au(0). Figure 5a–c shows SEM images of titania nanobowls on Si(111) surfaces and gold nanoparticle-loaded titania nanobowls after gold deposition. Scanning Auger microscopy (Figure 5d–f) was used to confirm the formation of metallic gold on the titania: four different sites were chosen for analysis, with sites 1–3 inside the pit regions and site 4 on the flat surfaces outside of the pits. Strong Au MNN signals were observed in sites 1–3, confirming the existence of gold, but only an extremely weak signal was observed from site 4 on the silica/silicon interface, indicating that gold deposition primarily occurred on the titania.

Gold Deposition on Etched Silicon Surface *via* Galvanic Displacement. Since the freshly etched nanopits on silicon are $Si-H_x$-terminated, whereas the surface remains coated with a more inert native oxide, the interiors of the nanopits should be amenable to electrochemistry. Galvanic displacement is a well-known electrochemical process, widely used for metal deposition on semiconductor surfaces.[91–99] In galvanic displacement, both the cathodic and anodic reactions occur simultaneously and spontaneously on H-terminated silicon surfaces and not on the insulating oxide interface.[91,92,100,101] Metal ions in solution are reduced by electrons from the silicon substrate lattice, resulting in the formation of metal particles or films on the surface. The resulting substrate oxidation causes the formation of a thin layer of SiO_x in the case of silicon substrates. As illustrated in Figure 6, $HAuCl_4$ can be spontaneously reduced to gold on silicon surfaces in the absence of any external electron source because of the overall positive cell potential. Metal deposition proceeds until *in situ* formation of the dielectric SiO_x layer blocks

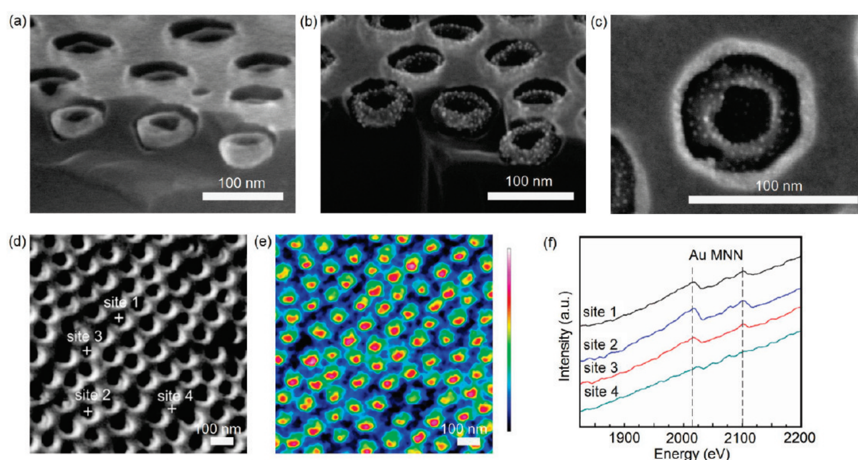

Figure 5. SEM images of (a) titania nanobowls on Si(111) surfaces and (b, c) gold nanoparticle-decorated titania nanobowls. (d) SEM image of a titania/gold-coated silicon surface taken with scanning Auger microscopy. (e) Ti LMM SAM and (f) gold Auger MNN signals of the four different sites chosen from (d).

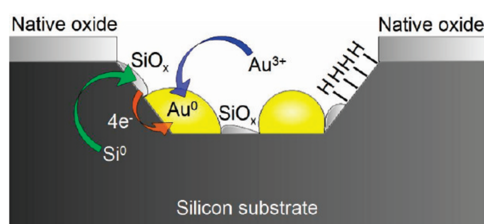

Figure 6. Schematic diagram of the galvanic displacement reaction of metal on silicon. Galvanic displacement takes place in the Si−H_x-terminated regions and is accompanied by *in situ* formation of SiO_x.

the electron transfer process. While it is unclear where the SiO_x layer is formed, it would be reasonable to assume that it would be in close proximity to the deposited metal.[102]

When a freshly etched silicon surface was immersed in a 10^{-4} M $HAuCl_4$ ethanolic solution for 5 min, as shown schematically in Figure 7a, and rinsed thoroughly with ethanol and water, strongly adhering nanoparticles of gold grew inside the etch pits; no metal was observed on the exterior flat surfaces (Figure 8a) that could not be removed with aggressive rinsing. The selective occurrence of galvanic displacement on the interior Si−H_x surfaces demonstrated the difference in chemical reactivity between the etch pit interior and the native oxide. The average size of the deposited gold nanoparticles was about 45 nm. Galvanic displacement did not continue any further with increased immersion times due to the absence of HF(aq) to dissolve the insulating SiO_2 that forms as the reaction proceeds; without HF(aq), the galvanic displacement reaction is self-limiting. The gold nanoparticles inside the etch pits were further characterized by scanning Auger microscopy, as shown in Figure 9. Figure 9b and c show the Auger maps of silicon and gold on the same scan area corresponding to that of the SEM image: Silicon (yellow-green) and gold (green) are clearly visualized at this spatial resolution. Figure 9d is the overlapped image of 9a−c, in which the green represents the gold and the blue represents the silicon. Figure 9e shows a SAM line profile along the red line, and the relative concentrations of gold and silicon along the line vary in an alternating manner, as expected.

In a second approach to utilize the SiH_x chemical handle within the etch pit interiors, the interiors were terminated with long alkyl chains to render them electrochemically inactive due to the insulating qualities of the organic monolayer, while the flat unetched top surfaces were hydride-terminated to enable galvanic displacement to occur in these areas, as outlined in Figure 7b. The areas of Si−H_x termination were functionalized *via* hydrosilylation of 1-octadecyne, producing Si-octadecenyl groups as was demonstrated in previous work.[31] Rinsing these samples with 1% HF(aq) to remove the native oxide on the top layer of the silicon transformed this interface into a Si−H_x-terminated surface. Subsequent immersion of this silicon wafer in a 10^{-4} M $HAuCl_4$ ethanolic solution for 5 min led to metal deposition exclusively on the top of the silicon wafer and not within the etch pit interiors. The insulating 1-octadecenyl layer prevented electron transfer from the silicon to the Au^{3+} salt, thus hindering the galvanic displacement reaction and gold deposition within the functionalized etch interior (Figure 8b).

As a control experiment, the silicon surface was rendered chemically homogeneous with Si−H_x groups, as outlined in Figure 7c. The freshly patterned and etched Si(100) wafer was terminated with Si−H_x groups in both etch pit interiors and on the top surface through immersion of a freshly etched sample in a 1% HF(aq) solution for 5 min. Exposure of this sample to the 10^{-4} M $HAuCl_4$ ethanolic solution for 5 min led to Au deposition in all regions of the substrate, as shown in Figure 8c, since all chemical differences between the silicon etch pit interiors and the top interface had been erased.

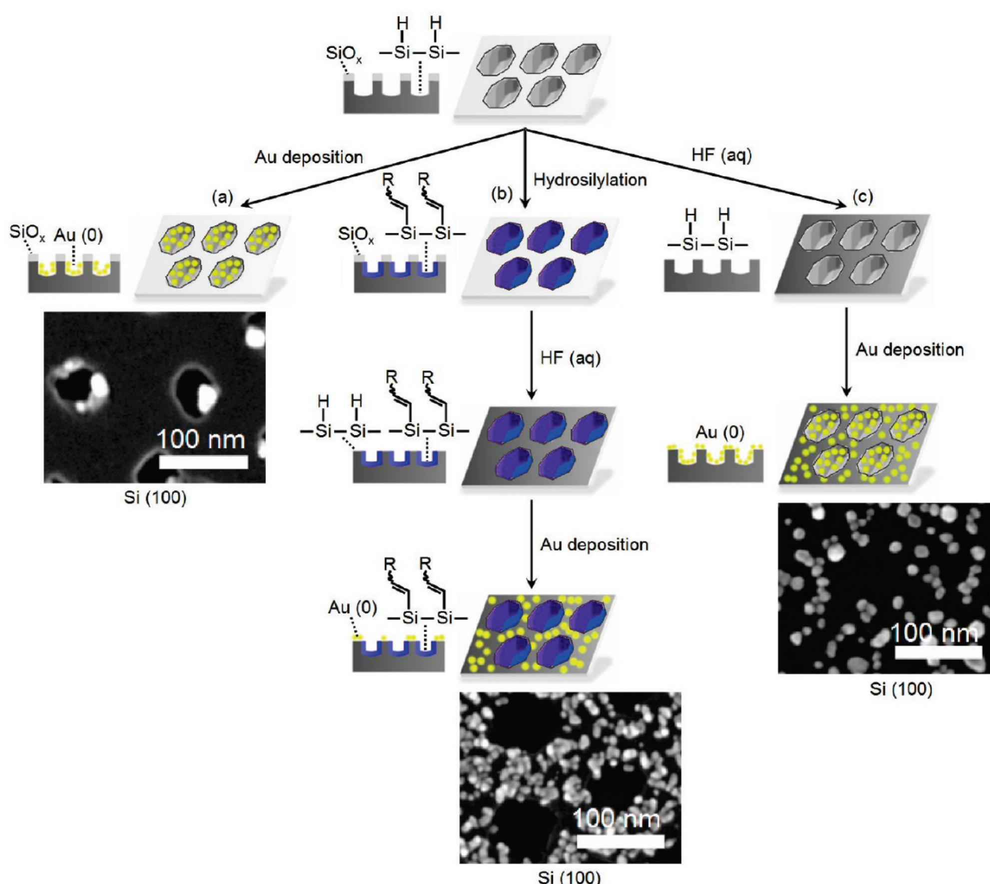

Figure 7. Schematic procedure for selective metal deposition on etched Si(100) surfaces: (a) inside the etched pits, (b) on the top flat silicon surface surrounding the etched pits, and (c) over the entire pit array (within the pits and on top surface).

CONCLUSIONS

In summary, we have demonstrated that silicon surfaces that have been etched with HF(aq) *via* a block copolymer template can be used as templates to pattern metallic and oxide nanostructures. Combined with approaches to achieve different chemical functionalizations on the interfaces, the etched silicon substrates provide the means to tune both shape and location of the synthesized nanostructures. The etched patterns may be a useful platform for the integration of a variety of other nanostructures with silicon surfaces.

EXPERIMENTAL METHODS

Materials. Asymmetric diblock copolymers of PS-*b*-P4VP were purchased from Polymer Source Inc. Hydrofluoric acid (HF) was purchased from J. T. Baker. Hydrogen tetrachloroaurate(III) trihydrate (Sigma Aldrich, 99.9%), titanium(IV) chloride (Alfa Aesar, 99.6%), octadecyltrichlorosilane (Sigma Aldrich, 90%), hydrogen peroxide (Fisher, 30%), sulfuric acid (J. T. Baker, 96.1%), ammonium hydroxide (J. T. Baker, 30%), hydrochloric acid (J. T. Baker, 36.5%), ethanol (Fisher, 99.8%), acetone (Fisher, 99.6%), hexane (Fisher, 99.8%), and toluene (Sigma Aldrich, 99.8%) were used in the preparations. Alkenes or alkynes (Aldrich) used for hydrosilylation were purified by distillation and stored in a refrigerator in an argon-filled glovebox. All other chemicals and solvents were used as received without further purification. High-purity water (18 MΩ·cm, Barnstead Nanopure water) was used throughout all experiments.

Analysis. Titania and gold structures on silicon were characterized by scanning electron microscopy, and Auger electron spectroscopy. The SEM images were taken with a Hitachi S-4800 FE-SEM in the National Institute for Nanotechnology (NINT). Auger electron spectroscopy was carried out on a JAMP-9500F field emission scanning Auger microprobe (JEOL Ltd.).

Silicon Cleaning Procedures. Prime-grade 4 in. diameter Si(100) and -(111) wafers were cut into approximately 1 by 1 cm^2 pieces. These silicon pieces were degreased in an ultrasonic bath of a common dish soap solution, rinsed in ultrapure water, and then dried by a stream of nitrogen gas. For cleaning, both standard piranha and RCA cleaning procedures were used.

1. Piranha Cleaning Procedure. A hot piranha solution (H_2SO_4/H_2O_2, 3:1, v/v) was prepared at 80 °C. The silicon wafers were immersed in the hot piranha solution for 30 min. After the wafers were removed from the solution and rinsed with water, they were dried in a nitrogen stream.

2. RCA Cleaning Procedure. The standard RCA clean involved two steps. In the first step, the silicon wafers were immersed in a hot solution of NH_4OH, H_2O_2, and Millipore water in a ratio of 1:1:5 at 80 °C for 20 min. The wafers were then rinsed with excess water and immersed in another hot solution of HCl, H_2O_2, and Millipore water in a ratio of 1:1:6 at 80 °C for 20 min. The wafers were then rinsed with water and dried in a nitrogen gas flow.

Polymer Template Preparation. The diblock copolymers, PS-*b*-P4VP (M_n = 109 000-*b*-27 000 g/mol), were weighed and dissolved in toluene at 80 °C by stirring overnight, followed by cooling to room temperature to make a ~1% w/w solution of

polymer micelles. A 1.2 × 10^{-2} mL volume of the block copolymer sample solution was then dropped onto the cleaned Si wafer and spin-coated for 1 min (spin coater model WS-400B-6NPP-Lite, Laurell Technologies, North Wales, PA) under argon to fabricate the thin films of polymer.

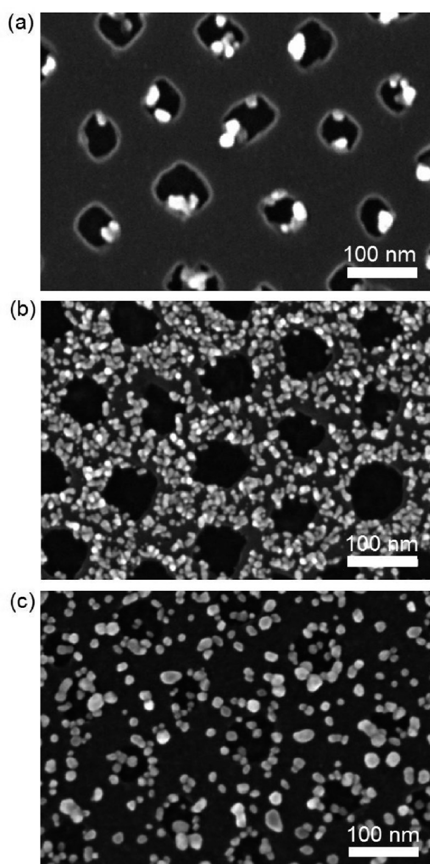

Figure 8. SEM images of gold nanoparticles (a) that form only within the etched pit interiors, (b) that decorate the top surface of the etched pit array, and (c) that decorate the entire surface with no selectivity for the pit interiors or the flat interface on Si(100) surfaces.

Fabrication of Etch Pit Arrays. The silicon wafer coated with PS-*b*-P4VP was immersed in a 0.02% HF aqueous solution for 40 min and then removed from the HF solution, rinsed with excess water, and dried with a nitrogen stream. The polymer residue was then removed with toluene.

Silanization and Oxidation of Silicon Surface. Freshly etched silicon substrates were placed in 20 mL of a 1.3 mM octadecyltrichlorosilane (CH_3-$(CH_2)_{17}SiCl_3$) (≥90%, Aldrich) solution in dry hexanes for 30 min at room temperature. The silanization reaction was carried out in glass containers. The silicon wafers were then removed from the self-assembly solution, transferred into 20 mL of neat hexane, and cleaned by ultrasonication for 3 min. The cleaning procedure was repeated three times, and the silicon wafers were then rinsed with dry hexanes and dried with nitrogen gas. After the silanization reaction, the samples were immersed in a 30% (w/w) hydrogen peroxide solution overnight at room temperature. The samples were then taken out from the oxidation solution, rinsed with water, and transferred into a three-neck flask without further drying.

Deposition and Release of Titania on Silicon Surface. To deposit titania exclusively in the etched pit interiors of oxidized wafers, the samples were removed from the 30% aqueous H_2O_2 solution, dried in air, rinsed with water, and then gently transferred into a water bath heated (80 °C) three-neck flask in which a rough vacuum was applied for 30 s. $TiCl_4$ vapor was then introduced into the flask from a liquid $TiCl_4$ source (room temperature) for 5 min. The sample was rinsed with water and dried in nitrogen gas after the TiO_2 deposition. In a control experiment, the freshly etched silicon shards were oxidized with the 30% hydrogen peroxide solution overnight at room temperature and transferred into the reaction container for titania deposition. Subsequently, the samples were thermally annealed at 550 °C in air for 3 h. The titania on silicon wafers can be further released from the surface by HF etching; the samples were immersed in a dilute HF solution [0.02% (aq)] for 6 h and then gently rinsed with water and dried in a nitrogen stream.

Gold Deposition on Titania. A gold growth solution was prepared by neutralizing a 10^{-5} M $HAuCl_4$(aq) solution to a pH of 7 using a 10^{-3} M KOH(aq) solution. The silicon wafers coated with titania were then immersed into the growth solution, and gold deposition was carried out for 5 min under a 5 W screen inspection UV lamp filtered to exclusively pass a narrow band around 254 nm.

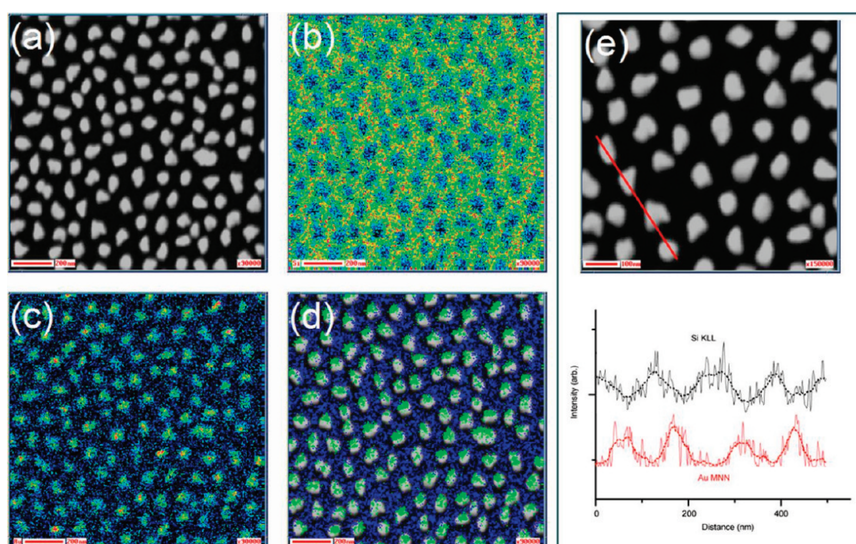

Figure 9. Scanning Auger microscopy images of gold nanoparticles on the etched Si(100) surface, prepared by galvanic displacement of gold nanoparticles: (a) SEM image; (b) Si KLL SAM; (c) Au MNN SAM; (d) overlapping images of (a), (b), and (c); (e) SAM line profiles of Si KLL (top) and Au MNN (bottom) along the red line marked in the SEM image (top) shown in (bottom). The scale bars are 200 nm in (a−d) and 100 nm in (e), respectively.

Hydrosilylation on Etched Silicon Surface. Thermal hydrosilylation of 1-octadecyne on etched silicon surfaces was carried out by immersing a freshly etched silicon substrate in a solution of 1-octadecyne in mesitylene (v/v = 1:3) under an argon atmosphere at 190 °C for 3 h. The substrate was then removed from the reaction solution, cleaned thoroughly with hexane and dichloromethane, and dried with nitrogen.

Deposition of Gold Nanoparticles on Etched Silicon Surface. The selective deposition of gold nanoparticles on etched silicon surfaces was carried out by galvanic displacement reactions. In the first experiment, the block copolymer on an as-prepared etched silicon substrate was removed *via* 5 min of ultrasonication in toluene, and the silicon substrate was immersed in a gold growth solution (10^{-4} M $HAuCl_4$ ethanolic solution, v_{water}:$v_{ethanol}$ = 1:1) for 5 min. The silicon substrate was then removed from the growth solution and rinsed thoroughly with ethanol and water. This procedure led to gold nanoparticle deposition in the pit interiors. In the second procedure, the silicon substrate with the 1-octadecenyl-terminated etch pit interiors was dipped into a 1% HF(aq) solution for 5 min to remove the native oxide layer. The substrate was removed from the HF solution, rinsed thoroughly with water, and then immersed in the gold growth solution for 5 min. The silicon substrate was then removed from the gold growth solution, rinsed with water and ethanol, and dried in nitrogen gas flow. This procedure enabled gold nanoparticles to be deposited selectively outside the etch pits. Third, as a control experiment, the freshly prepared silicon wafers with nanopatterned pits were immersed in a 1% HF(aq) solution for 6 min to remove the native oxide layer on the surface surrounding the pits. The silicon substrate was then dipped into the gold growth solution for 5 min, removed from the solution, rinsed with water and ethanol, and dried with nitrogen gas flow.

Acknowledgment. This research was supported by NSERC and NRC-NINT. L.X. thanks Southeast University for a sabbatical and the China Scholarship Council (CSC) for support. We are thankful for technical assistance provided at the National Institute for Nanotechnology (NINT), and we thank Dr. Dimitre Karpuzov and Shihong Xu at the Alberta Centre for Surface Engineering and Science (ACSES) for their assistance with scanning Auger microscopy and XPS.

Supporting Information Available: X-ray diffraction patterns of as prepared and annealed titania and additional SEM and SAM images of prepared structures on silicon. This material is available free of charge *via* the Internet at http://pubs.acs.org.

REFERENCES AND NOTES

1. Black, C. T. Polymer Self-Assembly as a Novel Extension to Optical Lithography. *ACS Nano* **2007**, *1*, 147–150.
2. Zabetakis, D.; Dressick, W. J. Selective Electroless Metallization of Patterned Polymeric Films for Lithography Applications. *ACS Appl. Mater. Interfaces* **2009**, *1*, 4–25.
3. Simeone, F. C.; Albonetti, C.; Cavallini, M. Progress in Micro- and Nanopatterning via Electrochemical Lithography. *J. Phys. Chem. C* **2009**, *113*, 18987–18994.
4. Carter, K. R. An Age-Old Printing Process Goes Nano. *ACS Nano* **2010**, *4*, 595–598.
5. Gao, Y.; Koumoto, K. Bioinspired Ceramic Thin Film Processing: Present Status and Future Perspectives. *Cryst. Growth Des.* **2005**, *5*, 1983–2017.
6. Chabinyc, M. L.; Salleo, A. Materials Requirements and Fabrication of Active Matrix Arrays of Organic Thin-Film Transistors for Displays. *Chem. Mater.* **2004**, *16*, 4509–4521.
7. Barth, J. V.; Costantini, G.; Kern, K. Engineering Atomic and Molecular Nanostructures at Surfaces. *Nature* **2005**, *437*, 671–679.
8. Gates, B. D.; Xu, Q.; Stewart, M.; Ryan, D.; Willson, C. G.; Whitesides, G. M. New Approaches to Nanofabrication: Molding, Printing, and Other Techniques. *Chem. Rev.* **2005**, *105*, 1171–1196.
9. Cheng, J. Y.; Ross, C. A.; Smith, H. I.; Thomas, E. L. Templated Self-Assembly of Block Copolymers: Top-Down Helps Bottom-Up. *Adv. Mater.* **2006**, *18*, 2505–2521.
10. Whitesides, G. M.; Grzybowski, B. Self-Assembly at All Scales. *Science* **2002**, *295*, 2418–2421.
11. Buriak, J. M. Organometallic Chemistry on Silicon and Germanium Surfaces. *Chem. Rev.* **2002**, *102*, 1271–1308.
12. Sieval, A. B.; Linke, R.; Zuilhof, H.; Sudhölter, E. J. R. High-Quality Alkyl Monolayers on Silicon Surfaces. *Adv. Mater.* *12*, 1457−1460.
13. Palmer, L. C.; Stupp, S. I. Molecular Self-Assembly into One-Dimensional Nanostructures. *Acc. Chem. Res.* **2008**, *41*, 1674–1684.
14. Kale, T. S.; Klaikherd, A.; Popere, B.; Thayumanavan, S. Supramolecular Assemblies of Amphiphilic Homopolymers. *Langmuir* **2009**, *25*, 9660–9670.
15. Ziener, U. Self-Assembled Nanostructures of Oligopyridine Molecules. *J. Phys. Chem. B* **2008**, *112*, 14698–14717.
16. Black, C. T.; Ruiz, R.; Breyta, G.; Cheng, J. Y.; Colburn, M. E.; Guarini, K. W.; Kim, H.-C.; Zhang, Y. Polymer Self Assembly in Semiconductor Microelectronics. *IBM J. Res. Dev.* **2007**, 605–633.
17. Hamley, I. W. Nanostructure Fabrication Using Block Copolymers. *Nanotechnology* **2003**, *14*, R39–R54.
18. Hayward, R. C.; Pochan, D. J. Tailored Assemblies of Block Copolymers in Solution: It Is All about the Process. *Macromolecules* **2010**, *43*, 3577–3584.
19. Bang, J.; Jeong, U.; Ryu, D. Y.; Russell, T. P.; Hawker, C. J. Block Copolymer Nanolithography: Translation of Molecular Level Control to Nanoscale Patterns. *Adv. Mater.* **2009**, *21*, 4769–4792.
20. Wiley, B. J.; Qin, D.; Xia, Y. Nanofabrication at High Throughput and Low Cost. *ACS Nano* **2010**, *4*, 3554–3559.
21. Merkel, T. J.; Herlihy, K. P.; Nunes, J.; Orgel, R. M.; Rolland, J. P.; DeSimone, J. M. Scalable, Shape-Specific, Top-Down Fabrication Methods for the Synthesis of Engineered Colloidal Particles. *Langmuir* **2010**, *26*, 13086–13096.
22. Sanchez, C.; Boissière, C.; Grosso, D.; Laberty, C.; Nicole, L. Design, Synthesis, and Properties of Inorganic and Hybrid Thin Films Having Periodically Organized Nanoporosity. *Chem. Mater.* **2008**, *20*, 682–737.
23. Giacomelli, C.; Schmidt, V.; Aissou, K.; Borsali, R. Block Copolymer Systems: From Single Chain to Self-Assembled Nanostructures. *Langmuir* **2010**, *26*, 15734–15744.
24. Park, C.; Yoon, J.; Thomas, E. L. Enabling Nanotechnology with Self Assembled Block Copolymer Patterns. *Polymer* **2003**, *44*, 6725–6760.
25. Fasolka, M.; Mayes, A. Block Copolymer Thin Films: Physics and Applications. *Annu. Rev. Mater. Res.* **2001**, *31*, 323–355.
26. Segalman, R. A. Patterning with Block Copolymer Thin Films. *Mater. Sci. Eng. R* **2005**, *48*, 191–226.
27. Hamley, I. W. Nanotechnology with Soft Materials. *Angew. Chem., Int. Ed.* **2003**, *42*, 1692–1712.
28. Darling, S. B. Directing the Self-Assembly of Block Copolymers. *Prog. Polym. Sci.* **2007**, *32*, 1152–1204.
29. Ouk Kim, S.; Solak, H. H.; Stoykovich, M. P.; Ferrier, N. J.; de Pablo, J. J.; Nealey, P. F. Epitaxial Self-Assembly of Block Copolymers on Lithographically Defined Nanopatterned Substrates. *Nature* **2003**, *424*, 411–414.
30. Cheng, J. Y.; Ross, C. A.; Thomas, E. L.; Smith, H. I.; Vancso, G. J. Fabrication of Nanostructures with Long-Range Order Using Block Copolymer Lithography. *Appl. Phys. Lett.* **2002**, *81*, 3657.
31. Qiao, Y.; Wang, D.; Buriak, J. M. Block Copolymer Templated Etching on Silicon. *Nano Lett.* **2007**, *7*, 464–469.
32. Aizawa, M.; Buriak, J. M. Block Copolymer-Templated Chemistry on Si, Ge, InP, and GaAs Surfaces. *J. Am. Chem. Soc.* **2005**, *127*, 8932–8933.
33. Aizawa, M.; Buriak, J. M. Nanoscale Patterning of Two Metals on Silicon Surfaces Using an ABC Triblock Copolymer Template. *J. Am. Chem. Soc.* **2006**, *128*, 5877–5886.
34. Chai, J.; Buriak, J. M. Using Cylindrical Domains of Block Copolymers To Self-Assemble and Align Metallic Nanowires. *ACS Nano* **2008**, *2*, 489–501.

35. Mizuno, H.; Buriak, J. M. Catalytic Stamp Lithography for Sub-100 nm Patterning of Organic Monolayers. *J. Am. Chem. Soc.* **2008**, *130*, 17656–17657.
36. Jackson, E. A.; Hillmyer, M. A. Nanoporous Membranes Derived from Block Copolymers: From Drug Delivery to Water Filtration. *ACS Nano* **2010**, *4*, 3548–3553.
37. Bang, J.; Jeong, U.; Ryu, D. Y.; Russell, T. P.; Hawker, C. J. Block Copolymer Nanolithography: Translation of Molecular Level Control to Nanoscale Patterns. *Adv. Mater.* **2009**, *21*, 4769–4792.
38. Park, S.-Y.; Sul, W.-H. The Effects of the Selectivity of the Toluene/Ethanol Mixture on the Micellar and the Ordered Structures of an Asymmetric Poly(Styrene-b-4-Vinylpyridine). *Polymer* **2008**, *49*, 3327–3334.
39. Spatz, J. P.; Mössmer, S.; Hartmann, C.; Möller, M.; Herzog, T.; Krieger, M.; Boyen, H.-G.; Ziemann, P.; Kabius, B. Ordered Deposition of Inorganic Clusters from Micellar Block Copolymer Films. *Langmuir* **2000**, *16*, 407–415.
40. Glass, R.; M ller, M.; Spatz, J. P. Block Copolymer Micelle Nanolithography. *Nanotechnology* **2003**, *14*, 1153–1160.
41. Glass, R.; Arnold, M.; Blümmel, J.; Küller, A.; Möller, M.; Spatz, J. P. Micro-Nanostructured Interfaces Fabricated by the Use of Inorganic Block Copolymer Micellar Monolayers as Negative Resist for Electron-Beam Lithography. *Adv. Funct. Mater.* **2003**, *13*, 569–575.
42. Ranzinger, J.; Krippner-Heidenreich, A.; Haraszti, T.; Bock, E.; Tepperink, J.; Spatz, J. P.; Scheurich, P. Nanoscale Arrangement of Apoptotic Ligands Reveals a Demand for a Minimal Lateral Distance for Efficient Death Receptor Activation. *Nano Lett.* **2009**, *9*, 4240–4245.
43. Cho, H.; Park, H.; Park, S.; Choi, H.; Huang, H.; Chang, T. Development of various PS-b-P4VP Micellar Morphologies: Fabrication of Inorganic Nanostructures from Micellar Templates. *J. Colloid Interface Sci.* **2011**, *356*, 1–7.
44. Kim, H.-C.; Park, S.-M.; Hinsberg, W. D. Block Copolymer Based Nanostructures: Materials, Processes, and Applications to Electronics. *Chem. Rev.* **2010**, *110*, 146–177.
45. Simon, P. F. W.; Ulrich, R.; Spiess, H. W.; Wiesner, U. Block Copolymer−Ceramic Hybrid Materials from Organically Modified Ceramic Precursors. *Chem. Mater.* **2001**, *13*, 3464–3486.
46. Jung, Y. S.; Ross, C. A. Orientation-Controlled Self-Assembled Nanolithography Using a Polystyrene−Polydimethylsiloxane Block Copolymer. *Nano Lett.* **2007**, *7*, 2046–2050.
47. Black, C. T. Self-Aligned Self Assembly of Multi-Nanowire Silicon Field Effect Transistors. *Appl. Phys. Lett.* **2005**, *87*, 163116.
48. Haberkorn, N.; Lechmann, M. C.; Sohn, B. H.; Char, K.; Gutmann, J. S.; Theato, P. Templated Organic and Hybrid Materials for Optoelectronic Applications. *Macromol. Rapid Commun.* **2009**, *30*, 1146–1166.
49. Fisher, A.; Kuemmel, M.; Järn, M.; Linden, M.; Boissière, C.; Nicole, L.; Sanchez, C.; Grosso, D. Surface Nanopatterning by Organic/Inorganic Self-Assembly and Selective Local Functionalization. *Small* **2006**, *2*, 569–574.
50. Park, H. J.; Kang, M.-G.; Guo, L. J. Large Area High Density Sub-20 nm SiO_2 Nanostructures Fabricated by Block Copolymer Template for Nanoimprint Lithography. *ACS Nano* **2009**, *3*, 2601–2608.
51. Tokuhisa, H.; Hammond, P. T. Nonlithographic Micro- and Nanopatterning of TiO_2 Using Polymer Stamped Molecular Templates. *Langmuir* **2004**, *20*, 1436–1441.
52. Chuang, V. P.; Gwyther, J.; Mickiewicz, R. A.; Manners, I.; Ross, C. A. Templated Self-Assembly of Square Symmetry Arrays from an ABC Triblock Terpolymer. *Nano Lett.* **2009**, *9*, 4364–4369.
53. Davis, R. J.; Liu, Z. Titania−Silica: A Model Binary Oxide Catalyst System. *Chem. Mater.* **1997**, *9*, 2311–2324.
54. Nijhuis, T. A.; Makkee, M.; Moulijn, J. A.; Weckhuysen, B. M. The Production of Propene Oxide: Catalytic Processes and Recent Developments. *Ind. Eng. Chem. Res.* **2006**, *45*, 3447–3459.
55. Shankar, K.; Basham, J. I.; Allam, N. K.; Varghese, O. K.; Mor, G. K.; Feng, X.; Paulose, M.; Seabold, J. A.; Choi, K.-S.; Grimes, C. A. Recent Advances in the Use of TiO_2 Nanotube and Nanowire Arrays for Oxidative Photoelectrochemistry. *J. Phys. Chem. C* **2009**, *113*, 6327–6359.
56. Di Valentin, C.; Pacchioni, G.; Selloni, A. Reduced and n-Type Doped TiO_2: Nature of Ti^{3+} Species. *J. Phys. Chem. C* **2009**, *113*, 20543–20552.
57. Chen, X.; Mao, S. S. Titanium Dioxide Nanomaterials: Synthesis, Properties, Modifications, and Applications. *Chem. Rev.* **2007**, *107*, 2891–2959.
58. Kanta, A.; Sedev, R.; Ralston, J. Preparation of Silica-on-Titania Patterns with a Wettability Contrast. *Langmuir* **2005**, *21*, 5790–5794.
59. Michel, R.; Reviakine, I.; Sutherland, D.; Fokas, C.; Csucs, G.; Danuser, G.; Spencer, N. D.; Textor, M. A Novel Approach To Produce Biologically Relevant Chemical Patterns at the Nanometer Scale: Selective Molecular Assembly Patterning Combined with Colloidal Lithography. *Langmuir* **2002**, *18*, 8580–8586.
60. Michel, R.; Lussi, J. W.; Csucs, G.; Reviakine, I.; Danuser, G.; Ketterer, B.; Hubbell, J. A.; Textor, M.; Spencer, N. D. Selective Molecular Assembly Patterning: A New Approach to Micro- and Nanochemical Patterning of Surfaces for Biological Applications. *Langmuir* **2002**, *18*, 3281–3287.
61. Lussi, J. W.; Michel, R.; Reviakine, I.; Falconnet, D.; Goessl, A.; Csucs, G.; Hubbell, J. A.; Textor, M. A Novel Generic Platform for Chemical Patterning of Surfaces. *Prog. Surf. Sci.* **2004**, *76*, 55–69.
62. Chinthamanipeta, P. S.; Lou, Q.; Shipp, D. A. Periodic Titania Nanostructures Using Block Copolymer Templates. *ACS Nano* **2011**, *5*, 450−456.
63. Matsushita, S. I.; Miwa, T.; Tryk, D. A.; Fujishima, A. New Mesostructured Porous TiO_2 Surface Prepared Using a Two-Dimensional Array-Based Template of Silica Particles. *Langmuir* **1998**, *14*, 6441–6447.
64. Chen, Y.; Park, S.-M.; Kim, H.-C.; McVittie, J. P.; Ting, C.; Nish, Y. Templated Electrochemical Synthesis of Titania Nanopillars on Conductive Substrates. *J. Electrochem. Soc.* **2010**, *157*, E155–E161.
65. Park, O.-H.; Cheng, J. Y.; Hart, M.; Topuria, T.; Rice, P. M.; Krupp, L. E.; Miller, R. D.; Ito, H.; Kim, H.-C. High Aspect-Ratio Cylindrical Nanopore Arrays and Their Use for Templating Titania Nanoposts. *Adv. Mater.* **2008**, *20*, 738–742.
66. Crossland, E. J. W.; Nedelcu, M.; Ducati, C.; Ludwigs, S.; Hillmyer, M. A.; Steiner, U.; Snaith, H. J. Block Copolymer Morphologies in Dye-Sensitized Solar Cells: Probing the Photovoltaic Structure−Function Relation. *Nano Lett.* **2009**, *9*, 2813–2819.
67. Li, X.; Zhang, L.; Wang, Y.; Yang, X.; Zhao, N.; Zhang, X.; Xu, J. A Bottom-Up Approach To Fabricate Patterned Surfaces with Asymmetrical TiO_2 Microparticles Trapped in the Holes of Honeycomblike Polymer Film. *J. Am. Chem. Soc.* **2011**, *133*, 3736−3739.
68. Peters, R. D.; Nealey, P. F.; Crain, J. N.; Himpsel, F. J. A Near Edge X-ray Absorption Fine Structure Spectroscopy Investigation of the Structure of Self-Assembled Films of Octadecyltrichlorosilane. *Langmuir* **2002**, *18*, 1250–1256.
69. Wang, R.; Parikh, A. N.; Beers, J. D.; Shreve, A. P.; Swanson, B. Nonequilibrium Pattern Formation in Langmuir-Phase Assisted Assembly of Alkylsiloxane Monolayers. *J. Phys. Chem. B* **1999**, *103*, 10149–10157.
70. Li, D.; Moore, L. W.; Swanson, B. I. Formation of Metal Clusters on the Surfaces of Covalently Bound Self-Assembled Ligand Monolayers. *Langmuir* **1994**, *10*, 1177–1185.
71. Howland, M. C.; Sapuri-Butti, A. R.; Dixit, S. S.; Dattelbaum, A. M.; Shreve, A. P.; Parikh, A. N. Phospholipid Morphologies on Photochemically Patterned Silane Monolayers. *J. Am. Chem. Soc.* **2005**, *127*, 6752–6765.
72. Patankar, N. A. Mimicking the Lotus Effect: Influence of Double Roughness Structures and Slender Pillars. *Langmuir* **2004**, *20*, 8209–8213.

73. Barthlott, W.; Neinhuis, C. Purity of the Sacred Lotus, or Escape from Contamination in Biological Surfaces. *Planta* **1997**, *202*, 1–8.
74. Hazlett, R. D. Fractal Applications: Wettability and Contact Angle. *J. Colloid Interface Sci.* **1990**, *137*, 527–533.
75. Spori, D. M.; Drobek, T.; Zürcher, S.; Ochsner, M.; Sprecher, C.; Mühlebach, A.; Spencer, N. D. Beyond the Lotus Effect: Roughness Influences on Wetting over a Wide Surface-Energy Range. *Langmuir* **2008**, *24*, 5411–5417.
76. Morita, M.; Ohmi, T.; Hasegawa, E.; Teramoto, A. Native Oxide Growth on Silicon Surface in Ultrapure Water and Hydrogen Peroxide. *Jpn. J. Appl. Phys.* **1990**, *29*, L2392–L2394.
77. Moreno, J. D.; Guerrero-Lemus, R.; M.Martínez-Duart, J.; Marcos, M. L.; González-Velasco, J. The Origin of Electroluminescence at Porous p-Silicon Layers-Electrolyte Interfaces. *Adv. Mater.* **1998**, *10*, 38–42.
78. Barrelet, C. J.; Robinson, D. B.; Cheng, J.; Hunt, T. P.; Quate, C. F.; Chidsey, C. E. D. Surface Characterization and Electrochemical Properties of Alkyl, Fluorinated Alkyl, and Alkoxy Monolayers on Silicon. *Langmuir* **2001**, *17*, 3460–3465.
79. Cheng, J.; Robinson, D. B.; Cicero, R. L.; Eberspacher, T.; Barrelet, C. J.; Chidsey, C. E. D. Distance Dependence of the Electron-Transfer Rate Across Covalently Bonded Monolayers on Silicon. *J. Phys. Chem. B* **2001**, *105*, 10900–10904.
80. Wang, X. D.; Graugnard, E.; King, J. S.; Wang, Z. L.; Summers, C. J. Large-Scale Fabrication of Ordered Nanobowl Arrays. *Nano Lett.* **2004**, *4*, 2223–2226.
81. Gu, W.; Tripp, C. P. Role of Water in the Atomic Layer Deposition of TiO_2 on SiO_2. *Langmuir* **2005**, *21*, 211.
82. Schrijnemakers, K.; Impens, N. R. E. N.; Vansant, E. F. Deposition of a Titania Coating on Silica by Means of the Chemical Surface Coating. *Langmuir* **1999**, *15*, 5807–5813.
83. Wang, T.-H.; Navarrete-López, A. M.; Li, S.; Dixon, D. A.; Gole, J. L. Hydrolysis of $TiCl_4$: Initial Steps in the Production of TiO_2. *J. Phys. Chem. A* **2010**, *114*, 7561–7570.
84. Haukka, S.; Lakomaa, E.-L.; Suntola, T. Analytical and Chemical Techniques in the Study of Surface Species in Atomic Layer Epitaxy. *Thin Solid Films* **1993**, *225*, 280–283.
85. Zhang, M.; Gao, G.; Zhao, D.; Li, Z.; Liu, F. Crystallization and Photovoltaic Properties of Titania-Coated Polystyrene Hybrid Microspheres and Their Photocatalytic Activity. *J. Phys. Chem. B* **2005**, *109*, 9411–9415.
86. Yin, Y.; Lu, Y.; Gates, B.; Xia, Y. Synthesis and Characterization of Mesoscopic Hollow Spheres of Ceramic Materials with Functionalized Interior Surfaces. *Chem. Mater.* **2001**, *13*, 1146–1148.
87. Ohno, T.; Sarukawa, K.; Matsumura, M. Photocatalytic Activities of Pure Rutile Particles Isolated from TiO_2 Powder by Dissolving the Anatase Component in HF Solution. *J. Phys. Chem. B* **2001**, *105*, 2417–2420.
88. Chan, S. C.; Barteau, M. A. Preparation of Highly Uniform Ag/TiO_2 and Au/TiO_2 Supported Nanoparticle Catalysts by Photodeposition. *Langmuir* **2005**, *21*, 5588–5595.
89. Hidalgo, M. C.; Maicu, M.; Navío, J. A.; Colón, G. Effect of Sulfate Pretreatment on Gold-Modified TiO_2 for Photocatalytic Applications. *J. Phys. Chem. C* **2009**, *113*, 12840–12847.
90. Kydd, R.; Scott, J.; Teoh, W. Y.; Chiang, K.; Amal, R. Understanding Photocatalytic Metallization of Preadsorbed Ionic Gold on Titania, Ceria, and Zirconia. *Langmuir* **2010**, *26*, 2099–2106.
91. Porter, L. A.; Choi, H. C.; Ribbe, A. E.; Buriak, J. M. Controlled Electroless Deposition of Noble Metal Nanoparticle Films on Germanium Surfaces. *Nano Lett.* **2002**, *2*, 1067–1071.
92. Magagnin, L.; Maboudian, R.; Carraro, C. Gold Deposition by Galvanic Displacement on Semiconductor Surfaces: Effect of Substrate on Adhesion. *J. Phys. Chem. B* **2002**, *106*, 401–407.
93. Sayed, S. Y.; Buriak, J. M. Epitaxial Growth of Nanostructured Gold Films on Germanium via Galvanic Displacement. *ACS Appl. Mater. Interfaces* **2010**, *2*, 3515–3524.
94. Sayed, S. Y.; Wang, F.; Malac, M.; Meldrum, A.; Egerton, R. F.; Buriak, J. M. Heteroepitaxial Growth of Gold Nanostructures on Silicon by Galvanic Displacement. *ACS Nano* **2009**, *3*, 2809–2817.
95. Ferralis, N.; Maboudian, R.; Carraro, C. Structure and Morphology of Annealed Gold Films Galvanically Displaced on the Si(111) Surface. *J. Phys. Chem. C* **2007**, *111*, 7508–7513.
96. Warren, S.; Reitzle, A.; Kazimirov, A.; Ziegler, J. C.; Bunk, O.; Cao, L. X.; Renner, F. U.; Kolb, D. M.; Bedzyk, M. J.; Zegenhagen, J. A Structure Study of the Electroless Deposition of Au on Si(1 1 1):H. *Surf. Sci.* **2002**, *496*, 287–298.
97. Magagnin, L.; Bertani, V.; Cavallotti, P. L.; Maboudian, R.; Carraro, C. Selective Deposition of Gold Nanoclusters on Silicon by a Galvanic Displacement Process. *Microelectron. Eng.* **2002**, *64*, 479–485.
98. Lv, S.; Suo, H.; Zhou, T.; Wang, C.; Jing, S.; Fu, Q.; Xu, Y.; Zhao, C. Effect of Synthesis Route on the Morphologies of Silver Nanostructures by Galvanic Displacement Reaction. *Solid State Commun.* **2009**, *149*, 227–230.
99. Ye, X. R.; Wai, C. M.; Zhang, D.; Kranov, Y.; McIlroy, D. N.; Lin, Y.; Engelhard, M. Immersion Deposition of Metal Films on Silicon and Germanium Substrates in Supercritical Carbon Dioxide. *Chem. Mater.* **2003**, *15*, 83–91.
100. Gao, D.; He, R.; Carraro, C.; Howe, R. T.; Yang, P.; Maboudian, R. Selective Growth of Si Nanowire Arrays via Galvanic Displacement Processes in Water-in-Oil Microemulsions. *J. Am. Chem. Soc.* **2005**, *127*, 4574–4575.
101. Porter, L. A.; Choi, H. C.; Schmeltzer, J. M.; Ribbe, A. E.; Elliott, L. C. C.; Buriak, J. M. Electroless Nanoparticle Film Deposition Compatible with Photolithography, Microcontact Printing, and Dip-Pen Nanolithography Patterning Technologies. *Nano Lett.* **2002**, *2*, 1369–1372.
102. Niwa, D.; Homma, T.; Osaka, T. Deposition Mechanism of Ni on Si(100) Surfaces in Aqueous Alkaline Solution. *J. Phys. Chem. B* **2004**, *108*, 9900–9904.